A Mobile App to Measure Facial Dimensions and Predict Respirator Size

Eric Elliott[1]*, Medhat Korna[1], Gregory Van Ermen[1], Daniel Barker[2], and John Lloyd[2]

[1] Technology Solutions Experts, Inc., 209 West Central Street, Suite 202, Natick, MA 01760, USA, USA
[2] Edgewood Chemical Biological Center, Research and Technology Directorate, ATTN: RDCB-DRP-R, Bldg. 3400, Aberdeen Proving Ground, MD 21010-5424, USA

* Corresponding author and E-mail: eric.elliott@tseboston.com

ABSTRACT

The current workflow for sizing military respirators is time consuming, manually intensive, and tedious, but is necessary due to the critical need for respirators to fit properly, especially in operating environments when Warfighters may be exposed to chemical, biological, radiological, and nuclear threats. To reduce the time and resource cost of the fitting process, Technology Solutions Experts, Inc. developed a software application to rapidly generate a 3D model of a user's face, accurately compute anthropometric measurements, and estimate the appropriate size of a respiratory protective mask. In this paper, we discuss implementing our 3D model generation and size prediction methodology in a mobile app, and collecting and analyzing data to measure the methodology's predictive capability. Our verification and validation results show that our current method for fit prediction is insufficient to replace traditional fit tests. However, there is evidence to suggest that face measurements obtained from 3D models can produce fit predictions as accurate as hand measurements but in a fraction of the time, and without subject matter expertise.

Keywords: Respirator, mask, fit, 3D, model, prediction, face, images, measurements, anthropometry

INTRODUCTION

Military respirators are critical to the survival of Soldiers who are exposed to chemical, biological, radiological and nuclear (CBRN) threats. The fit of the respirator on the wearer directly determines whether the respirator will effectively protect against foreign agents. Identifying the correct size of a full facepiece respirator for an individual requires specialized equipment for measuring aerosols within the mask, an operator trained to use the fit testing equipment and interpret its results, and the time and colocation of both operator and testing subject. The Chemical and Biological Defense (CBD) program seeks a quicker, less manually intensive, yet reliable method to select the correct respirators for individuals and to approximate the fit factor.

Through a Small Business Innovative Research (SBIR) grant, Technology Solutions Experts Inc. (TSE) developed a method to generate 3D head forms (3DHFs) from 2D images, estimate facial measurements, and to predict the appropriate size of the Avon C50 respirator for an individual using the estimated measurements. To deploy this methodology and make it available to a wide audience, we

developed MASQ (Mask Analysis and Size Quantification), a mobile app capable of running on common Android and iOS phones (shown in Figure 1). In this paper we present the results of our research and development, and an analysis of the predictive capabilities of the methodologies we developed for MASQ.

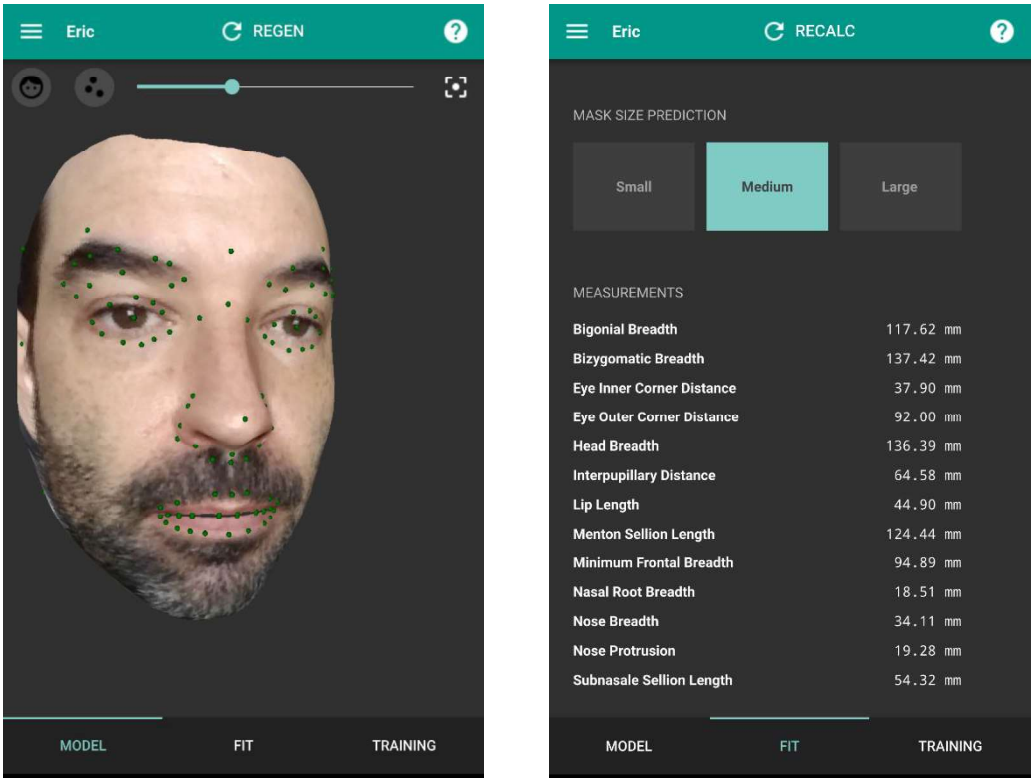

Figure 1. Screenshots of MASQ showing a generated 3D model (left), and estimated facial measurements (right).

Summary of Previous Work

We previously researched and developed a method to generate 3DHFs from 2D images and implemented a proof of concept application to demonstrate the feasibility of the approach. This work is detailed in a previous paper (Biagiotti, Korna, Rice, & Barker, 2019) and summarized here for background and context.

To generate 3D models, MASQ first detects a set of 68 facial landmarks on input images (shown in Figure 2) and then uses the landmarks to transform vertices on a base 3D model into a final 3D representation of the input images. MASQ uses a 3rd party open source C++ library called *eos* (Huber P. , A lightweight 3D Morphable Face Model fitting library in modern C++, 2016) to both estimate the locations of facial landmarks and to morph the corresponding vertices on the base model.

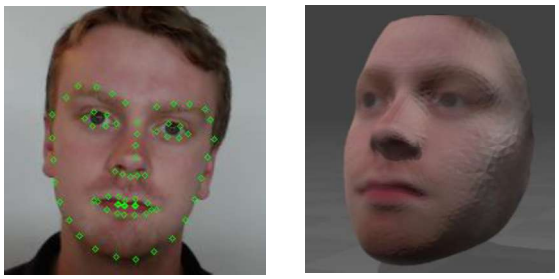

Figure 2. Example of landmark detection (left) and resulting 3D head form (right).

The *eos* library utilizes the Surrey Face Model (SFM), a 3D face model parameterized via principle component analysis (PCA) to identify the dimensions of highest variation. The SFM was constructed from a set of 169 head scans encompassing a broad set of demographics, though not necessarily representative of the U.S. military population. Table I lists the age and racial and breakdown of the subjects that were used to construct the SFM.

Table I. Demographics of Subjects Used to Construct the SFM

Age Group (years)	# of Subjects
0-19	9
20-29	106
30-44	33
45-59	13
60+	8
Perceived Race	**# of Subjects**
Caucasian	101
Black	10
Eastern Asian	34
South Asian, Arabic, or Latin American	24

For each set of input landmarks, MASQ estimates the pose angle of the face to properly orient the input landmarks, maps the 2D landmarks to their 3D counterparts on the base model, and extracts a texture from the source image to overlay on the final 3D model. Figure 2 shows an example of the final textured 3D head form constructed from the 2D image input.

MATERIALS AND METHODS

Our proof of concept relied on several manual steps, including identifying anthropometric landmarks (ALs) on generated 3DHFs, and converting facial dimensions from dimensionless model units to mm by measuring test subjects. To transition to a mobile device workflow we developed methods to automatically identify landmarks on 3D models and to compute measurements in mm without hand-measurements. We then implemented methods for improving accuracy of generated 3DHFs and finally performed a verification and validation (V&V) study to measure the performance of MASQ's facial measurement estimation and size prediction algorithms.

Identifying Landmarks on 3D Head Forms

In our proof of concept we used the Maya 3D authoring application to manually identify points on generated 3DHFs that corresponded to ALs of interest, and to compute linear distances between two landmarks to get facial dimension measurements. The landmarks that are used for face detection and 3D model generation are commonly used for face detection (Sagonas, Tzimiropoulos, Zafeiriou, & Pantic, 2013), but they don't necessarily correspond to the landmarks we use for facial measurement, so we needed a method to automate landmark identification and dimension measurement. We explored analyzing the structure of a generated model to identify regions and landmarks. For example, one could analyze the 3D triangle mesh to identify structures like eyes and lips, then locate the extents of the structures to identify eye and lip corners (Figure 3). However, many landmarks have more nuanced criteria for identification, which we determined would have led to unreliable placements.

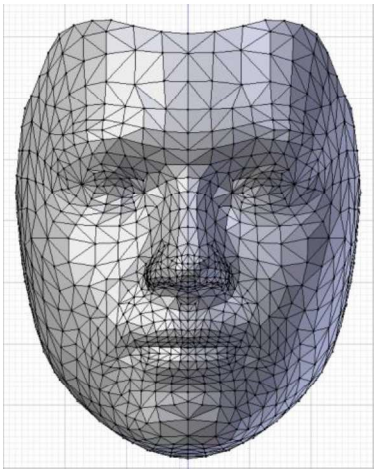

Figure 3. Surrey 7448 vertex morphable model.

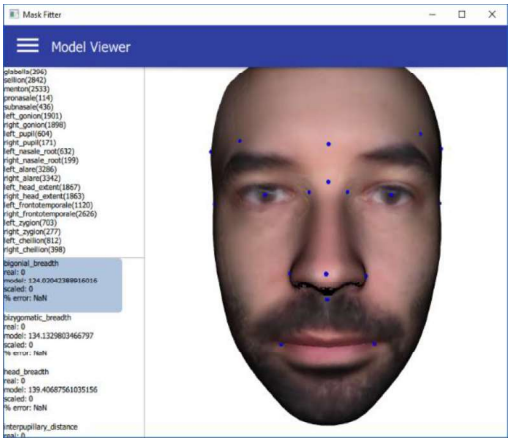

Figure 4. Model viewer showing locations of automatically detected ALs on a generated 3DHF.

Instead, we used the fact that the number and ordering of vertices in a generated model are the same as the base morphable model, only differing in their absolute positions. To make use of this, we manually identified the vertices on the base morphable model that corresponded to our landmarks of interest. This was a one-time process done via visual inspection to produce a mapping of vertex number to landmark. With this mapping, MASQ is able to find the vertex, and therefore the coordinates, of each landmark on a generated model automatically via a simple lookup (Figure 4).

Determining Scale from 2D Images

The 3DHFs that MASQ generates are dimensionless, so without additional information, there is no way to compute measurements in mm which is required for predicting mask size. To transform the 3DHF into mm, we first estimate a measurement in mm between two landmarks on a 2D image of the subject. We then use that distance and the corresponding distance in 3D model units to compute a ratio which is then used to scale the 3D model into mm.

Determining distances between landmarks in images requires either knowledge of photo parameters including the lens focal length, distance from lens to subject, and camera sensor size, or identifying an object in the image that has a known size. Because determining distance from lens to subject is difficult and imprecise, we developed a method for detecting an object of known dimension (OKD) in the image and using it to calculate the size in millimeters (mm) of a single pixel in the image by counting the width in pixels of the known object.

$$MMPerPixel = \frac{KnownObjectWidth_{mm}}{KnownObjectWidth_{px}}$$

Given a pixel size, we can then compute a distance in mm between any two points in the image. We use MASQ's landmark detection capabilities to identify the outer corners of the eyes and compute the eye outer corner (EOC) distance as the number of pixels from corner to corner, multiplied by the pixel size to get the distance in mm. While any facial dimension could be used as the reference measurement, the OKD should be located along the same linear path as the reference dimension in order to maximize accuracy. Holding an object to the eye corners achieves that goal while also being easy for the user to understand and accomplish.

$$EOC_{mm} = EOC_{px} * MMPerPixel$$

We then use the EOC distance in mm and the EOC distance in 3DHF units to derive the number of mm per 3DHF unit, thus allowing us to convert any measurement in 3DHF unit into mm.

$$MMPer3DHF = \frac{EOC_{mm}}{EOC_{3DHF}}$$

Known Object Detection and Measurement

Any object can be used for the purposes of this method, as long as its dimensions are known and consistent and it is placed on the same plane as the outer corners of the eyes. After evaluating numerous options, we selected the credit card as the OKD for initial implementation and subsequently added an additional option for using a custom shape, which produces results that are more reliable.

Credit Card Scaling

Most banking and ID cards conform to the ISO/IEC 7810 ID-1 standard (53.98mm x 85.60mm). Our approach combines Canny edge detection (Canny, 1986), Hough line detection (Matas, Galambos, & Kittler, 2000), and a ranking algorithm to identify the top and bottom lines of a credit card in an image, as seen in Figure 5. The distance between these lines is then measured in pixels. The real height of the card (53.98mm) is divided by the distance producing the mm/pixel ratio.

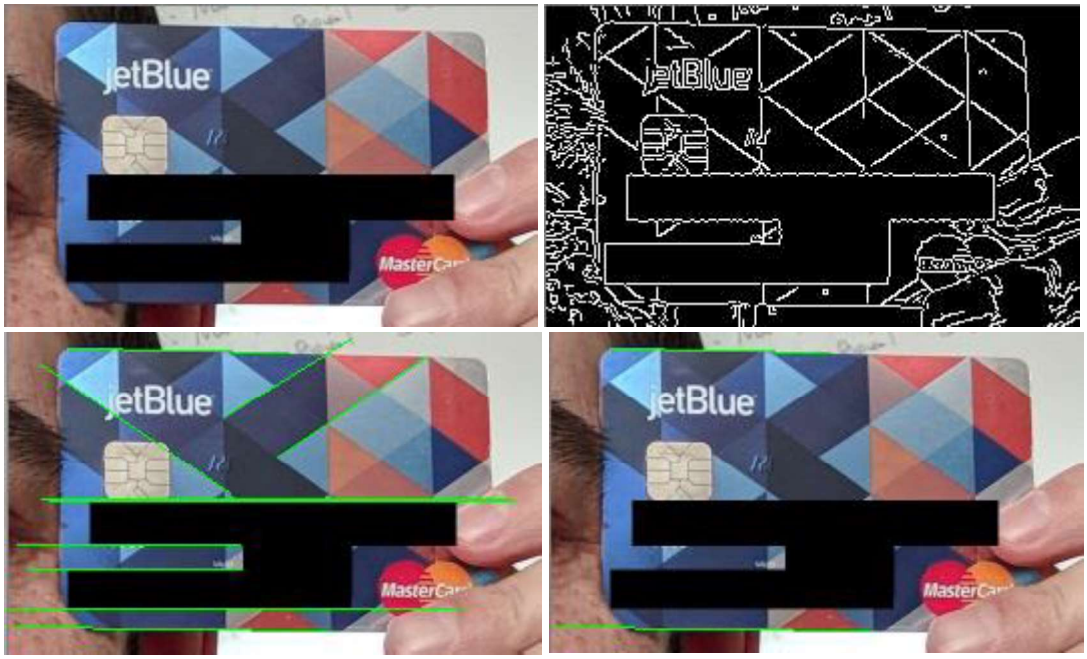

Figure 5. Scale calculation image processing from original image (top left), to Canny edge detection (top right), to Hough line detection (bottom left), and the final top and bottom lines by rank (bottom right).

Custom Scale Card

We found that identifying a credit card with potentially different colors and markings could be unreliable. Consequently, we experimented with using different shapes that can be more easily detectable. The downside of using a custom shape is that a user must print out the shape, but the improved detection reliability is substantial. Figure 6 shows a scaling image printed out on a business card and held next to the eyes just as with a credit card.

Using this shape allows us to use a simplified detection method that first translates the image to black and white, and then finds a continuous region of black pixels that matches the known height/width ratio of the black rectangle on the predefined image. Instead of using edge detection to find the extents of the black square, MASQ uses the contour detection functions provided by OpenCV to find all of the curves that are continuous, non-overlapping sets of pixels of the same color. Once detected, curves that don't have bounding rectangles matching the ratio of the scaling card, and those that are too small a percentage of the overall image are excluded. The remaining contour is then shown to the user to confirm detection was successful. While we didn't perform rigorous automated testing, we manually tested both credit card and scaling card detection in many different lighting and background conditions. From this it was clear that the scaling card resulted in far fewer failed or incorrect detections, faster detections, and better accuracy.

Figure 6. Scaling card held next to eyes to provide reference scale.

Improving Model Accuracy

In an effort to improve the accuracy of generated 3D models, we explored the benefits of using a higher resolution morphable model, increasing the number of landmarks detected per 2D image, and modifying various parameters in the 3D generation process to identify optimal settings.

Model Resolution

In our proof of concept, we used the lowest resolution of the Surrey Face Model, consisting of 7448 vertices, as the basis for generating 3DHFs. We later acquired the high (29587 vertices) resolution model in order to test the benefits of increased vertex density on model generation accuracy. Figure 7 shows wireframe models of three resolutions of the SFM.

Although offering the potential for improved accuracy, additional vertices also lead to the potential for increased error. We found that the high-resolution model provided no benefit to model accuracy as any benefit of increased resolution was offset by any inaccuracies being equally magnified. The high-resolution model also resulted in a substantial increase in processing time, and as a result we chose to use the low-resolution model until new methods are developed to improve 2D landmark and pose detection. We anticipate that combining the high resolution model with perfectly accurate 2D landmark detection would improve overall accuracy but we have not tested that hypothesis.

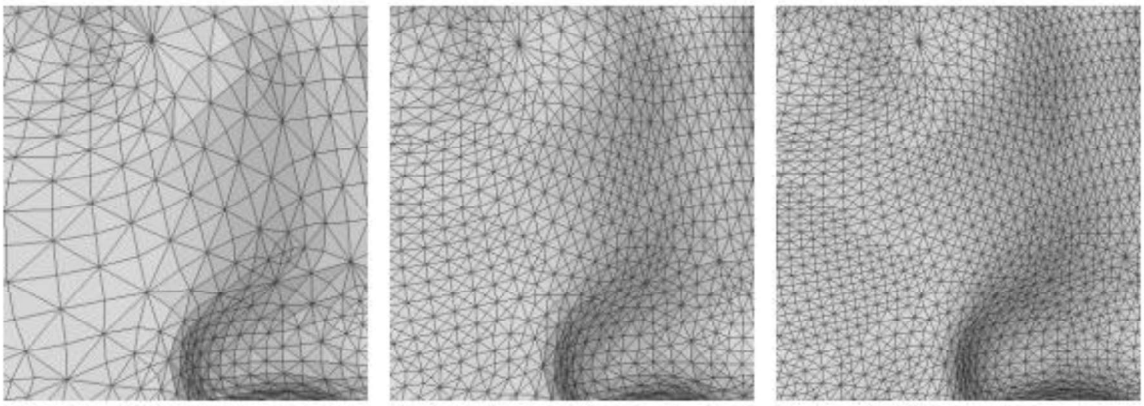

Figure 7. Morphable model resolutions (from left to right): 3448 vertices, 16758 vertices, 29587 vertices.

Landmark Density

Another method to improve model generation accuracy is to detect and map more points on the input images. To increase the number of landmarks used for transforming the morphable model, we trained a new landmark detection model using 103 landmarks instead of the original 68. To train and test the new detection model, we obtained the Helen dataset (Le, 2017), which consists of face images from the photo sharing website Flickr, annotated with landmarks to locate the eyes, nose, mouth, eyebrows, and jawline. An example of the detected landmarks is shown in Figure 8. When compared with landmarks from Figure 2, additional landmarks around the brows and nose can be observed, as well additional landmark density in the lips, eyes, and jawline.

We updated MASQ to support configuration of the landmark detection model in order to facilitate testing with both the original 68-landmark model and the 103-landmark model. As with increasing the morphable model resolution, the added landmark density also introduces potential for new errors. Since 3D model accuracy is dependent on the accuracy of 2D landmark detection and location, the increased

number of landmarks means there is more opportunity to introduce errors. While we didn't measure the accuracy of 2D landmark detection using 68 and 103 landmarks independently, we did test the final 3D headform accuracy when using each option. The landmark detection model is just one of many configurable options that we tested, with results for various configurations shown in section 4.

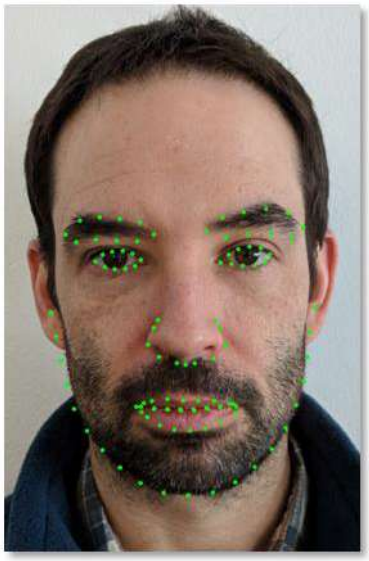

Figure 7. Subject annotated with 103 detected landmarks.

Parameter Configuration

In addition to model resolution and landmark density, we explored how the number and pose angle of images used to generate the model impacted model accuracy. The model can utilize multiple images of the same subject to refine the PCA parameters that define the final 3D headform. More images can both improve or degrade accuracy, largely dependent on how accurately landmarks are located on the 2D images. As the angle between the camera and the subjects facing direction, which we refer to as the pose angle, deviates from 0 degrees (facing the camera) to -90 degrees or 90 degrees (left or right profile), accuracy of landmark location tends to decrease. To filter out images that may result in inaccurate landmarks, we specify a configurable maximum pose angle (MPA). However, the pose angle is computed based on the detected landmarks, so filtering out potentially inaccurate landmarks is dependent on a measurement derived from those same landmarks. While not ideal, at worst it will include some images that should have been excluded, as opposed to excluding good images. To explore what parameters produced the best results, we tested a variety configurations of model resolution, landmark density, image count, and maximum pose angle. The results of these experiments are shown in section 4.

Verification and Validation

To verify and validate the algorithms used by the MASQ app, we employed an independent expert in anthropometry and fit testing to collect data on a set of subjects. For each subject, fit tests were administered for the Avon C50 respirator, anthropometric dimensions were hand-measured, and photos and videos were taken. Using these data, we measured the accuracy of 2D image scale estimates, facial dimension estimates, and mask size predictions produced by the MASQ algorithms.

Data Collection Protocol

To select subjects and perform data collection, we employed Anthrotech Inc., (https://anthrotech.net/), an independent company with expertise in anthropometry and fit testing. Anthrotech collected data for 36 subjects, with facial measurements distributed across a previously developed fit panel (Zhuang, Bradtmiller, & Shaffer, New Respirator Fit Test Panels Representing the Current U.S. Civilian Workforce, 2007).

Subjects were measured using procedures outlined in the *Measurer's Handbook: U.S. Army Anthropometric Survey* (Clauser, Tebbetts, Bradtmiller, McConville, & Gordan, 1987-1988), by one of two experts with extensive knowledge and background in identifying landmarks and measuring the identified dimensions. Each dimension was measured once using common measurement equipment, including sliding and spreading calipers, while the subject was either standing or sitting.

For each subject, five different types of data were recorded:

1. Facial measurements for 12 facial dimensions: Bigonial Breadth, Bizygomatic Breadth, Eye Outer Corner Distance, Head Breadth, Interpupillary Distance, Lip Length, Menton-Sellion Length, Minimum Frontal Breadth, Nasal Root Breadth, Nose Breadth, Nose Protrusion, Subnasale-Sellion Length
2. A forward facing image of the subject with a 2D scaling card held to the side of their face
3. A ~10 second video of the subject's head as they rotated from one side to the other
4. A fit test score produced by following the OSHA standard fit test protocol (OSHA Standards) for up to 3 different sizes (S, M, L) of the Avon C50 respirator
5. Basic demographic data including sex, age, height, weight.
    a. This data was not used in this study, we collected in case it may prove useful in future research to refine the model.

2D Image Scale Estimation

For each of the 36 subjects, we used MASQ to estimate the eye outer corner (EOC) distance based on an image of the subject holding a scaling card, as described in section 3.2. We then computed the error of the estimation as:

$$EOC_{err} = \frac{|EOC_{est} - EOC_{real}|}{EOC_{real}}$$

Where,

EOC_{err}: $Eye\ Outer\ Corner\ distance\ error$

EOC_{real}: $Measured\ distance\ in\ mm\ between\ eye\ outer\ corners$

EOC_{est}: $Estimated\ distance\ in\ mm\ between\ eye\ outer\ corners\ computed\ from\ scaling\ card$

Facial Dimension Estimation

To compute facial dimension measurements, we used MASQ to generate a 3D model of the subject's head from a set of 2D images extracted from the video of the subject rotating their head from side to side. The generated 3D model is made up of dimensionless vertices, and each measurement is a dimensionless distance between two 3D points. To convert to millimeters, we used the estimated EOC distance discussed in section 3.4.2 to derive a scaling factor as described in section 3.2. For each subject, we applied the scaling factor to compute a measurement in mm for each of the 12 dimensions, and then computed the measurement error for each dimension as:

$$M_{err} = \frac{|M_{est} - M_{real}|}{M_{real}}$$

Where,

M_{err}: $Estimated\ measurement\ error$

M_{est}: $Estimated\ measurement$

M_{real}: $Real\ measurement$

We then computed the average error across all dimensions for each subject, the average error across all subjects for each dimension, and an aggregate error across all subjects and dimensions. We applied this analysis multiple times using models generated with a variety of configuration parameters (see Table I for a listing of model generation cases) to identify settings that produced the best results.

Mask Size Prediction

Each subject was fit with at least one of each of the three sizes (Small, Medium, and Large) of the Avon C50. The OSHA standard fit test methodology (OSHA Standards) was followed to produce a fit score by measuring aerosols inside and outside the mask in various postures and various facial expressions. A score of at least 500 was considered passing, and if multiple sizes resulted in a passing score, the highest score was used as the best fit.

To predict mask size, MASQ uses distributions from both a bivariate fit panel, based on face height and face width, and a PCA fit panel (Zhuang, et al., 2008) that takes into account ten different facial measurements. MASQ uses measurements derived from the generated 3D model to identify the cell of each fit panel that the subject falls into. Based on data correlating fit panel cells and respirator size (Zhuang, et al., 2008), each fit panel cell is associated with a percentage of subjects that fit a particular size. MASQ selects the size with the maximum fit percent from both the bivariate and PCA fit panels. It uses the size selected from the PCA panel cell unless the subject did not fit within any cell, in which case it uses the size associated with the bivariate panel cell. In the case that the subject falls below the threshold of both fit panels, size small is predicted, and if the subject falls above the threshold, size large is predicted. While a small number of subjects did fall outside the bounds of the fit panel measurement thresholds, it wasn't specifically recorded as it is just another indication of measurement estimation inaccuracy which is already captured.

To measure accuracy we compared the size predicted by the MASQ algorithm with the size determined by the fit test to produce a percent accuracy, calculated as the number of size matches divided by the number of tests. We measured accuracy multiple times using models generated with a variety of configuration parameters (see Table I for a listing of model generation cases) to identify settings that produced the best results. Since our goal was to replicate the mask size recommendation resulting from the fit-testing process, we did not consider whether MASQ predicted a size that had a passing fit-test score, however this may be worth exploring in the future.

RESULTS

Figure 9 shows the percent error of EOC measurements derived from the scale card image for each subject. The average error was 5.19%, and the median error was 4.00%.

Figure 10 is a plot of the average accuracy of measurement estimates, and the average accuracy of size predictions for all subjects when using measurements derived from eight model generation configurations. The eight cases presented were based on observations of parameters that produced reliable results across all phases of the model generation process and were selected to provide a sampling of possible combinations. Also included are two control cases, the MEAN case, which used the unmodified morphable model for all subjects, and the MEASURED case, which used the hand-measurements instead of estimating measurements from a 3D model. The Measurement Estimate accuracy in Figure 10 is computed by calculating the accuracy of each individual dimension estimate as a percentage of the hand-measurement, then taking the average of all accuracies. The sizing accuracy is computed by calculating the percentage of subjects for which the predicted size matched the size recommended by the subject's fit test. For each model generation case, four configuration parameters were varied:

1. **Model Resolution**: Either the low-resolution or high-resolution SFM
2. **Number of Input Images**: The number of input images used to construct the 3D model
3. **Maximum Pose Angle (MPA)**: The maximum allowable deviation from center of a subjects facing angle
4. **Landmarks Detected**: Either the 68 or 103 landmark detection model

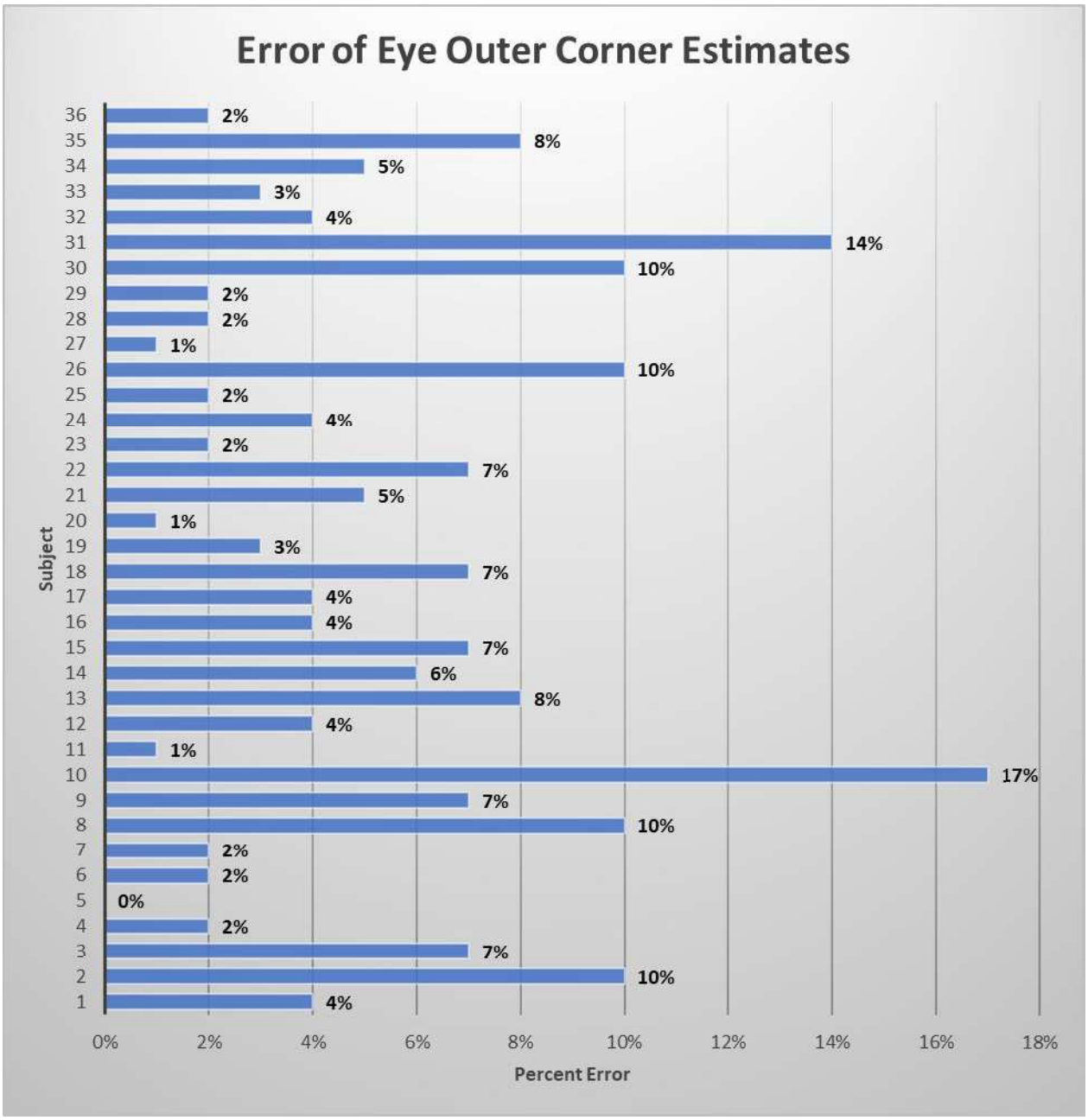

Figure 9. EOC estimate errors relative to hand-measured values for each subject.

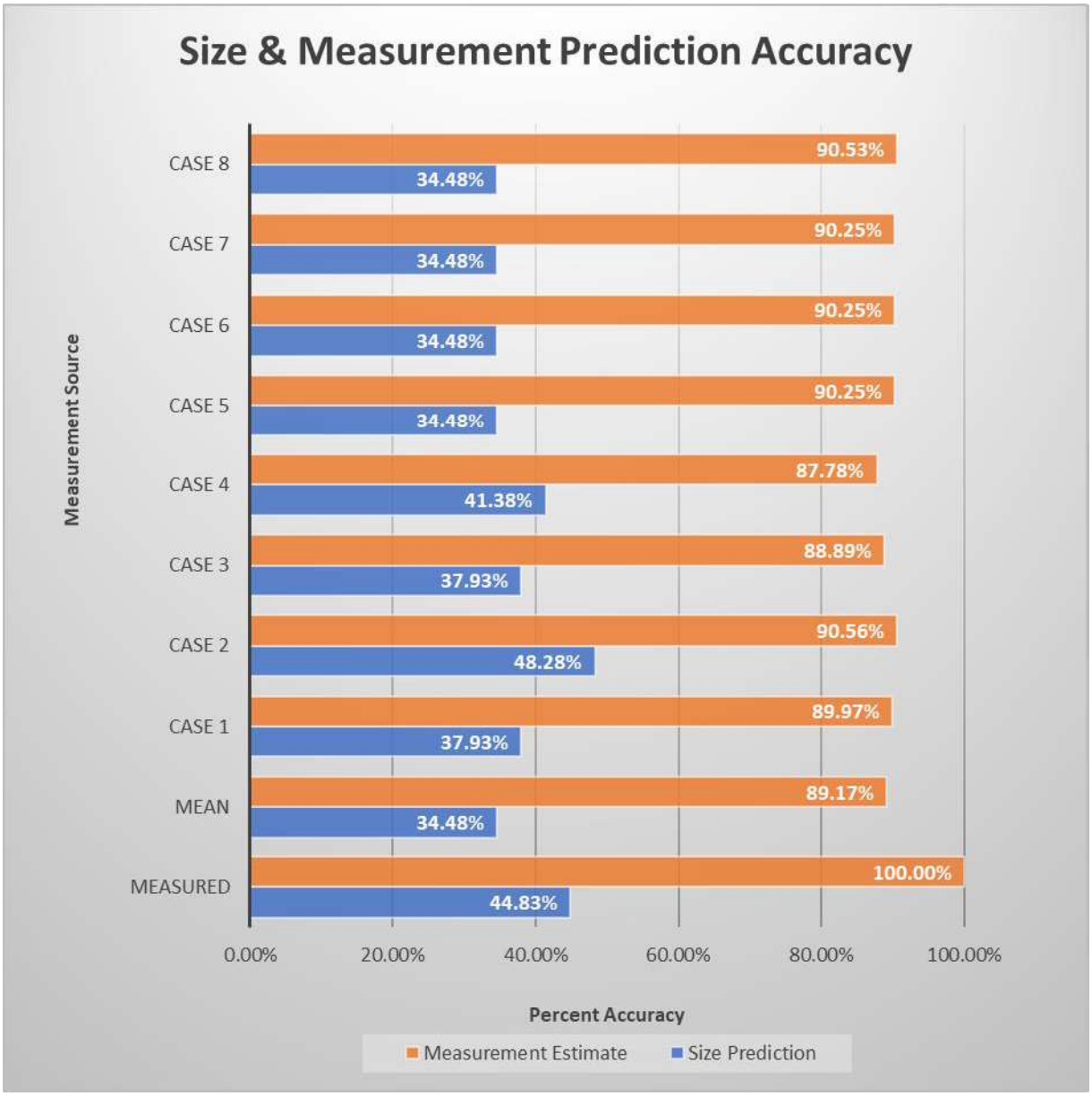

Figure 10. Average percent accuracy of measurement estimates and size predictions across all subjects for eight different model generation cases and two control cases.

Table II describes the specific model generation parameters used for cases 1 through 8.

Table II. Descriptions of Test Cases (each case includes the resolution of the model used, the number of images used to generate the model, the max. pose angle for input images, and the number of landmarks detected for each image)

Measurement Source	Model Resolution	# Input Images	Max.Pose Angle	Landmarks Detected
CASE 1	Hi-res	1	n/a	68
CASE 2	Low-res	1	n/a	68
CASE 3	Low-res	1	n/a	103
CASE 4	Low-res	12	+/- 10 degrees	103
CASE 5	Low-res	20	+/- 5 degrees	68
CASE 6	Low-res	20	+/- 10 degrees	68
CASE 7	Low-res	20	+/- 20 degrees	68
CASE 8	Low-res	100	+/- 20 degrees	68

Sources of Error

Estimated measurement error comes from three primary sources, landmark detection, 3D model morphing, and scale calculation. We have not independently measured landmark detection or orientation accuracy, however it could be done by manually annotating images with landmarks as the source of ground truth and comparing with the automatically detected locations. Similarly, 3D model morphing has not been independently measured, and doing so is more difficult as it would require a source of ground truth for landmarks in 3D space, such as a high resolution scan. Scaling card accuracy is presented in Figure 8, with error being introduced from automated detection of the EOC landmarks, placement of the scaling card either in front of or behind the line connecting EOC landmarks, orientation of the scaling card that is not parallel to the camera, and measurement of the height and width in pixels of the black square on the scaling card within the image.

CONCLUSIONS

Conclusions of the Verification and Validation

From the V&V study, we found that size prediction using the best-case scenario of hand-measured facial dimensions produced an accuracy rate of 45%. This result indicates a shortcoming of the size prediction methodology and that using fit-panel correlation does not produce sufficiently accurate predictions to replace fit-tests.

However, model generation case 2 (see figure 9) produced the most accurate size predictions (48%), even performing better than the hand-measured case. While better performance than hand-measured values is likely an anomaly, it does indicate that predicting size via model generation can perform just as well as hand-measurement. This result indicates that if an algorithm that predicts mask sizes given hand-measured dimensions can be developed, then MASQ model generation could be a viable replacement for the time and resource intensive hand-measurement process.

Also of note is that case 2 performed better than cases that used more images for model generation. Although the goal of additional images is to refine the model to better conform to the subject's face, it in fact seems to introduce error. Initial tests show that as the pose angle increases, the probability

that landmarks that are inaccurately detected increases. While filtering out images beyond the MPA threshold aims to mitigate this issue, it can be unreliable because it relies on computing the pose angle after landmarks have been detected. In many cases, even when a face is beyond the MPA threshold, the model erroneously detects landmarks that do fall with within the MPA threshold, merging them into the final model and reducing accuracy.

MASQ Application

MASQ is an easy to use mobile app for generating customized 3D head forms for individuals, estimating facial measurements, and predicting respirator size. While size prediction is still lacking, MASQ offers additional features not described in this paper that make it a useful tool for individuals, as well as researchers. MASQ supports multi-user operation and online data storage, making it a useful tool for conducting studies and collecting measurement and model data. For individuals, it features a tool to analyze hairlines and detect potential interference with mask seals, and it includes a guided training workflow to ensure users not only use a properly sized mask, but also understand how to properly inspect, don, and tighten their protective equipment. MASQ currently operates on the Android and iOS platforms, however it is not yet generally available.

Future Work

The data collected as part of the MASQ V&V can provide a useful resource for further investigation and model development. By pairing multi-angle images with facial measurements, the V&V data set contains useful information that has previously been unavailable, enabling insights that are not possible with simple linear measurements alone. To make use of these data, we suggest further research to find correlations between facial data and fit-test results. Specifically, we believe a machine-learning approach that is based on multiple dimensions of facial data, including linear measurements, contours, images, and 3D models is likely to provide the most benefit. Although the data collected for this V&V effort are a good start, a successful machine-learning model will likely require more data points, so we suggest a follow-on data collection effort with the goal of collecting measurements, videos, and fit-tests for an additional 100 to 200 subjects. After training and validating a model with the enhanced data set, it could then replace the existing fit-panel-based prediction algorithm while still using MASQ's existing dimensional analysis and 3D model generation capabilities to provide the model inputs.

Another area of future improvement is the scale calculation. Although the scaling card method is accurate in the ideal situation, it is prone to user error, particularly if the card is held significantly in front of or behind the eyes, or held at a severe angle. It can also be cumbersome, and requires printing the image. One option to investigate is the use of technologies integrated into the latest smart phones for the purposes of augmented reality (AR). Apple's ARKit application programming interface (API) supports methods for measuring objects by tracking relative motion in camera frames over time. A combination of landmark detection combined with these measurement capabilities could provide a scale calculation that is both accurate, automatic, and requires no user intervention.

The Avon C50 was selected as the first mask to investigate as it is a commonly used military respirator and was selected by the project sponsor. Exploring fit prediction for masks that are commonly used by the civilian population, such as the N95, is another avenue of future research. MASQ could be adapted to any mask which depends on proper size selection for optimal effectiveness, however, further data collection that pairs facial dimension measurements with proper sizing is first required.

Acknowledgements

The research and development described in this paper was funded by SBIR grants sponsored by the Chemical and Biological Defense program of the U.S. Department of Defense. The V&V data

collection was performed by Anthrotech Inc. and masks used for subject fit testing were supplied by Avon Protection.

REFERENCES

Biagiotti, E., Korna, M., Rice, D. O., & Barker, D. (2019). Predicting respirator size and fit from 2D images. *International Journal of Human Factors Modelling and Simulation*.

Canny, J. (1986). A Computational Approach to Edge Detection. *IEEE Trans. on Pattern Analysis and Machine Intelligence, 8(6)*, 679-698.

Clauser, C., Tebbetts, I., Bradtmiller, B., McConville, J., & Gordan, C. C. (1987-1988). *Measurer's Handbook: U.S. Army Anthropometric Survey.* Natick, Massachusetts: United States Army Research, Development, and Engineering Center.

Huber, P. (2016). *A lightweight 3D Morphable Face Model fitting library in modern C++*. Retrieved from https://github.com/patrikhuber/eos

Huber, P. (2017). *C++11 implementation of the supervised descent optimisation method*. Retrieved from https://github.com/patrikhuber/superviseddescent

Huber, P., Feng, Z., Christmas, W., Kittler, J., & Rätsch, M. (2015). Fitting 3D Morphable Models using Local Features. *IEEE International Conference on Image Processing (ICIP).* Quebec City.

Huber, P., Guosheng, H., Tena, R., Mortazavaian, P., Koppen, W. P., Christmas, W., . . . Kittler, J. (2016). A Multiresolution 3D Morphable Face Model and Fitting Framework. *The 11th International Joint Conference on Computer Vision, Imaging and Computer Graphics Theory and Applications.* Rome.

(2015). *ISO/TS 16976-2.*

Le, V. (2017, December 27). *Helen Dataset*. Retrieved from http://www.ifp.illinois.edu/~vuongle2/helen/

Matas, J., Galambos, C., & Kittler, J. (2000). Robust Detection of Lines Using the Progressive Probabilistic Hough Transform. *Cimputer Vision and Image Understanding*, 119-137.

OpenCV Team. (n.d.). *OpenCV Library*. Retrieved 2017, from https://opencv.org/

OSHA Standards. (n.d.). *Appendix A to § 1910.134: Fit Testing Procedures*. Retrieved from Occupational Safety and Health Administration: https://www.osha.gov/pls/oshaweb/owadisp.show_document?p_id=9780&p_table=STANDARDS

Sagonas, C., Tzimiropoulos, G., Zafeiriou, S., & Pantic, M. (2013). 300 Faces in-the-Wild Challenge: The first facial landmark localization Challenge. *IEEE Int'l Conf. on Computer Vision (ICCV-W).* Sydney.

Zhuang, Z., & Bradtmiller, B. (2005). Head-and-face anthropometric survey of U.S. respirator users. *Journal of Occupational and Environmental Hygiene*, 567-576.

Zhuang, Z., Bradtmiller, B., & Shaffer, R. E. (2007). New Respirator Fit Test Panels Representing the Current U.S. Civilian Workforce. *Journal of Occupational and Environmental Hygeine*, 647-659.

Zhuang, Z., Groce, D., Ahler, H. W., Iskander, W., Landsittel, D., Guffey, S., . . . Shaffer, R. E. (2008). Correlation Between Respirator Fit and Respirator Fit Test Panel Cells by Respirator Size. *Journal of Occupational and Environmental Hygiene*, 617-628.

Zhuang, Z., Slice, D. E., Benson, S., Lynch, S., & Viscusi, D. J. (2010). Shape Analysis of 3D Head Scan Data for U.S. Respirator Users. *EURASIP Journal on Advances in Signal Processing, 2010: 248954*.